Electrochimica Acta 75 (2012) 191–200

Contents lists available at SciVerse ScienceDirect

Electrochimica Acta

journal homepage: www.elsevier.com/locate/electacta

Co-deposition of Pt and ceria anode catalyst in supercritical carbon dioxide for direct methanol fuel cell applications

Eunyoung You[a], Rolando Guzmán-Blas[b], Eduardo Nicolau[b], M. Aulice Scibioh[b], Christos F. Karanikas[a], James J. Watkins[c,*], Carlos R. Cabrera[b,*]

[a] Department of Chemical Engineering, University of Massachusetts, Amherst, MA 01003, USA
[b] Department of Chemistry and NASA Center for Advanced Nanoscale Materials, University of Puerto Rico, Rio Piedras Campus, PO Box 70377, San Juan, PR 00936-8377, USA
[c] Department of Polymer Science and Engineering, University of Massachusetts, Amherst, MA 01003, USA

ARTICLE INFO

Article history:
Received 29 December 2011
Received in revised form 28 February 2012
Accepted 25 April 2012
Available online 3 May 2012

Keywords:
Supercritical fluid deposition
Methanol oxidation
Platinum-ceria
Carbon dioxide
Thin-layer electrode
Direct methanol fuel cell

ABSTRACT

Pt and mixed Pt-ceria catalysts were deposited onto gas diffusion layers using supercritical fluid deposition (SFD) to fabricate thin layer electrodes for direct methanol fuel cells. Dimethyl (1,5-cyclooctadiene) platinum (II) ($CODPtMe_2$) and tetrakis (2,2,6,6-tetramethyl 3,5-heptanedionato) cerium (IV) ($Ce(tmhd)_4$) were used as precursors. Hydrogen-assisted Pt deposition was performed in compressed carbon dioxide at 60 °C and 17.2 MPa to yield high purity Pt on carbon-black based gas diffusion layers. During the preparation of the mixed Pt-ceria catalyst, hydrogen reduction of $CODPtMe_2$ to yield Pt catalyzed the deposition of ceria from $Ce(tmhd)_4$ enabling co-deposition at 150 °C. The catalyst layers were characterized using X-ray diffraction (XRD), X-ray photoelectron spectroscopy (XPS) and scanning electron microscope-energy dispersive spectral (SEM-EDS) analyses. Their electrochemical performance toward methanol oxidation was examined in half cell mode using a three electrode assembly as well as in fuel cell mode. The thin layer electrodes formed via SFD exhibited higher performance in fuel cell operations compared to those prepared by the conventional brush-paint method. Furthermore, the Pt-ceria catalyst with an optimized composition exhibited greater methanol oxidation activity than pure platinum.

1. Introduction

Low-temperature fuel cells are attractive power sources for portable and vehicular applications. Direct methanol fuel cells (DMFCs) are at the forefront of commercialization due to their favorable characteristics including high energy density, operation at near ambient conditions and low emissions. Moreover, methanol is a renewable fuel source and offers fast and convenient refueling, as it is a liquid from −97.0 to 64.7 °C [1,2].

Despite the attractiveness of DMFCs, hurdles exist in the effective lifetime of the electrodes. Pt, considered to be one of the best catalysts for the DMFCs, suffers from poisoning, especially at the anode side during the methanol electro-oxidation by carbon monoxide (CO) chemisorption, leading to a significant drop in the overall performance [3,4]. Efforts have been made to mitigate CO poisoning by the addition of other metals to platinum such as Ru [5–10], Mo [11,12], W [11,13], Sn [11], Ni [14–16], and Nb [17]. Among these combinations, binary Pt Ru alloys are still considered to be state of the art catalysts for methanol oxidation in DMFCs. The addition of transition metal oxides such as MoO_x, VO_x and WO_x to PtRu has also been evaluated for an enhanced methanol oxidation reaction [18–21]. These modified catalysts have been reported to yield a higher methanol oxidation current than the conventional PtRu catalysts. Ruthenium crossover [22], however, has triggered serious concerns about anode stability.

Yet another impediment for early DMFC commercialization is the high cost of noble metal catalysts employed in the electrodes. Attempts have been made to reduce the catalyst loading by increasing Pt utilization [22–26] using new fabrication methods to enhance the three-phase boundary.

The use of non-noble catalysts is another approach for electrode cost reduction. Yu et al. [27] incorporated an oxygen storage material such as ceria into the cathode catalyst to increase the local oxygen concentration and attained performance enhancement in the DMFC. Xu and Shen [28,29] reported that the electrochemical oxidation of methanol, ethanol, glycerol and ethylene glycol on Pt-CeO_2/C catalyst constructed in alkaline media showed improved performance compared to conventional Pt/C catalysts. Campos et al. [30] prepared Pt/CeO_2 catalyst layers on a glassy carbon electrode by occlusion deposition method using a bath containing both ceria and K_2PtCl_6. An increase in catalytic activity for methanol oxidation with the ceria composite electrode was found when compared to the Pt/C system. Yuan et al. [74] reported that carbon nano-

* Corresponding authors.
E-mail address: carlos.cabrera2@upr.edu (C.R. Cabrera).

0013-4686/$ – see front matter © 2012 Elsevier Ltd. All rights reserved.
http://dx.doi.org/10.1016/j.electacta.2012.04.091

tubes used as supports for platinum catalysts deposited with metal oxides(CeO_2, TiO_2, and SnO_2) were prepared for their application as anode catalyst in DMFC. Catalyst with the addition of CeO_2, TiO_2, and SnO_2 presented higher catalytic activity than pure platinum catalyst, and the catalysts with CeO_2 were the best among. Tang et al. [75] prepared $Pr_xCe_yO_z$(x/y = 3/1, 1/1, 1/3) modified Pt/C catalysts by wet precipitation and reduction method. The results showed that the Pt-($Pr_1Ce_1O_z$)/C catalyst had the highest catalyst activity, the best stability and CO-tolerante which could be used as a suitable electrocatalyst for direct methanol fuel cell. Lee and Manthiran [76] prepared Pt-CeO_2/C catalysts prepared by one-step syntheses of conventional borohydride reduction and reverse microemulsion methods. The results suggested the possibility of the Pt-CeO_2/C-based catalysts, which are more stable than PtRu/C and even Pt/C, as alterative anode catalysts for direct methanol fuel cell. Guo et al. [31] employed PtRu-CeO_2/C catalyst and found that a particular composition, namely $PtRu_{0.7}(CeO_2)_{0.3}$/C, yielded a higher methanol oxidation current than an unmodified PtRu/C catalyst. By wet-impregnation method, Scibioh et al. [23] prepared Pt-CeO_2/C catalyst and examined their methanol oxidation activity. They found that 40 wt% Pt-9 wt% CeO_2/C exhibited a better activity and stability than the unmodified 40 wt% Pt/C catalyst.

DMFC anode catalyst development requires not only the exploration of new catalyst materials, which includes noble and non-noble metals but also an innovative catalyst layer engineering to fabricate thin, efficient electrodes.

Supercritical fluid deposition (SFD) yields pure and conformal metal, metal oxide and alloy films on topographically complex surfaces with high deposition rates [32]. This combination of attributes is enabled by the physico-chemical properties of supercritical fluids (SCFs) including gas-like transport properties, liquid-like densities, and zero surface tension [33]. Compared to conventional liquid solvents, SCFs show enhanced mass transfer characteristics (low viscosities and high diffusivities) while having equivalent solvating properties. The absence of surface tension enables the complete wetting of surfaces. Carbon dioxide has been extensively used as the process fluid for the supercritical deposition of metal and metal oxide film depositions due to its easily accessible critical point (T_c = 31 °C, P_c = 7.376 MPa), low-cost, non-flammability and environmentally benign properties. Due to many organometallic compounds being soluble in SCFs, such as carbon dioxide, SFD provides orders of magnitude higher precursor concentrations than traditional vapor based deposition methods such as chemical vapor deposition (CVD). After the deposition, the reaction chamber is simply depressurized to remove the reaction byproducts to obtain high purity films [32]. Watkins, co-workers and others have deposited various metal films, such as Ag [34], Au [35,36], Co [37], Cu [33,38–42], Ni [33,37,43], Pd [36,44,45], Pt [36,46,47], Rh [36], Ru [48,49] and oxides of Al [50,51], Bi [52], Ce [52], Ga [51], Hf [52], Mn [50], Nb [52], Ru [50], Ta [52], Ti [52,53], Y [50,54], Zr [50,52] using supercritical CO_2. It has been demonstrated that in supercritical carbon dioxide ($scCO_2$), organometallic precursor, such as dimethyl (1,5-cyclooctadiene) platinum (II), can be readily reduced to yield high purity metal films on a Si wafer, organic substrates, and within aluminum oxide membranes [47]. O'Neil et al. carried out conformal deposition of various metal oxides, demonstrating that the oxide deposition is owing to the hydrolysis of the organometallic compounds in $scCO_2$ [52]. Other work has focused on the deposition of metal particles and films within porous inorganic supports [45] and the deposition of metal particles within polymers, including Teflon [47].

Recently, Lin et al. demonstrated preparing catalyst layers using SCF, particularly for use in DMFCs [55]. PtRu nanoparticles were deposited on carbon nanotubes in $scCO_2$ using a methanol co-solvent (20 vol%) and H_2 at 200 °C [56]. The catalyst was then mixed into a Nafion® solution to obtain a black suspension and an aliquot of this catalyst containing solution was dropped onto glassy carbon electrode surface. An and co-workers similarly prepared PtRu carbon nanotube nanocomposites using different metal precursors and dispersed the catalyst powder in N,N-dimethylformamide to generate a black suspension that was coated onto a glassy carbon electrode [57]. Jiang et al. impregnated Pd directly onto a Nafion® electrolyte membrane in supercritical CO_2 in order to reduce methanol crossover for DMFC [58]. It may be desirable to directly deposit thin catalyst layers on top of the gas diffusion layers (carbon paper) to replace the time- and labor-intensive ink paint-brushing process currently in use.

Here we report the deposition of Pt and Pt-ceria anode catalysts via SFD method directly onto gas diffusion layers and examined their activities for methanol oxidation in half cell and direct methanol fuel cell systems. Further, these catalysts layers were characterized using X-ray diffraction (XRD), X-ray photoelectron spectroscopy (XPS) and scanning electron microscope-energy dispersive X-ray fluorescence spectroscopy (SEM-EDS) techniques.

2. Experimental

2.1. Fabrication of electrode layers

2.1.1. Conventional brush-paint method

Gas diffusion layers (GDL) were made by coating Vulcan XC-72R (1 mg-cm^{-2}) onto teflonized carbon paper substrates (Toray TGPH-060, 20% PTFE). 5 mg of Vulcan XC-72R was mixed with 200 μl of nanopure water and a mixture of 1:1 methanol and 100 μl of 2-propanol and sonicated for 1 h to create a slurry. Then, 5 wt% Nafion® solution (Sigma–Aldrich) was added to the mixture to attain a 15 wt% polymer mixture. After sonication, the mixture was stirred overnight. The carbon coating was applied by spray-brushing the carbon ink over the oven-dried carbon paper substrates until an approximate loading of 1 mg-cm^{-2} of ink was achieved. After carbon coating, the electrodes are prepared for catalyst ink deposition. Thus, catalyst ink dispersions were prepared by mixing appropriate amounts of Pt-black (Johnson Matthey PLC, London, UK), de-ionized water, isopropyl alcohol, and 5 wt% Nafion® solution. The catalyst ink was brush-painted onto 5 cm^2 of carbon paper (3 mg-cm^{-2}). These brush-painted Pt-black electrodes were used as the cathodes and anode control during the course of this investigation in order to compare them with the gas-diffusion electrodes made by SFD (Section 2.1.2).

2.1.2. Supercritical fluid deposition method

Supercritical CO_2 deposition of Pt and ceria was performed on the GDLs, which were made as described in Section 2.1.1. The GDL was placed in a high pressure reactor with an internal volume of 25 ml. The reactor configuration is shown in Fig. 1a. The GDL was secured to the stage using, a stainless steel gasket, which has a square through hole resulting in an exposed area of ~5 cm^2. A known amount of metal precursor was put in the high pressure reactor and the reactor was sealed with a Viton® O-ring.

A schematic of the sample structures with the sample notations is shown in Fig. 1b along with the mass uptake in each layer after the serial depositions. The GDL was dried in an oven maintained at 110 °C for 10 min before and after the SFD and the weights were recorded. A typical SFD of the Pt layer used 0.05 mmol of dimethyl (1,5-cyclooctadiene) platinum (II) (Strem Chemicals, Newburyport, MA). The concentration of the precursor in $scCO_2$ at the reaction condition is at least an order of magnitude lower than its solubility limit reported in the literature [59]. The reactor and ancillary tubing were initially purged with N_2 while the reactor wall temperature was set and controlled at 60 °C for 1 h. Supercritical CO_2 was delivered via a 60 °C jacketed syringe pump (Teledyne ISCO

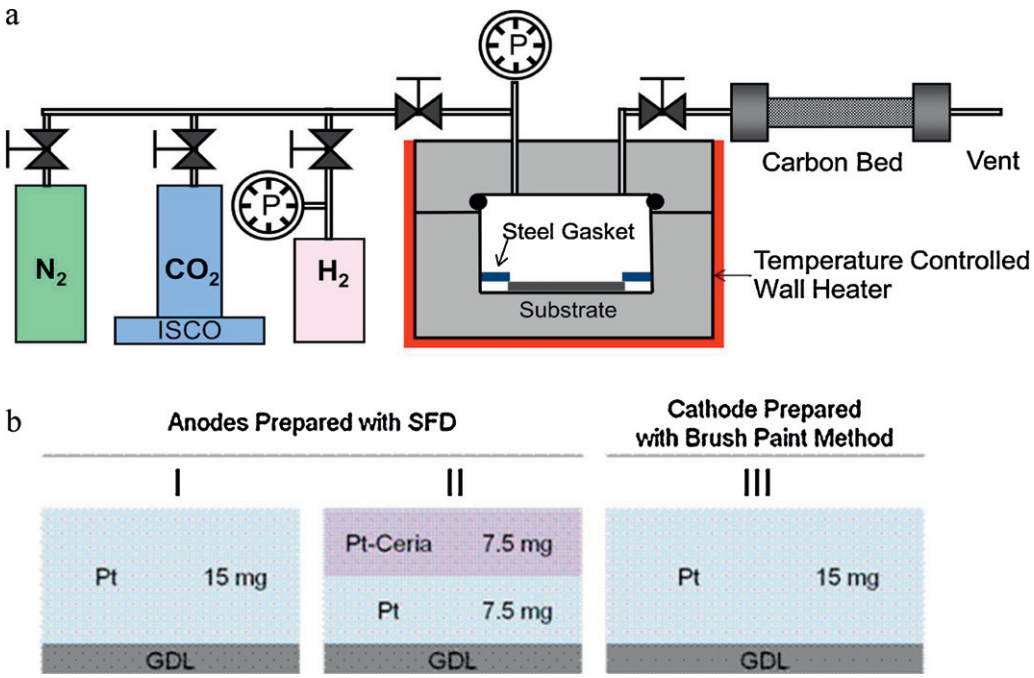

Fig. 1. (a) Schematic representation of the supercritical fluid deposition reactor set-up which was used for the preparation of the anode electrodes for the direct methanol fuel cells. (b) Anode catalyst samples prepared using supercritical fluid deposition and the cathode catalyst sample employed for the direct methanol fuel cell study. The active area of each electrode was 5 cm^2.

Inc. Lincoln, NE) and the reactor was pressurized to 17.2 MPa. The reactor was maintained at these conditions for 1 h to dissolve the precursor in CO_2. A 200% molar excess of H_2 was then dosed into the reactor to induce the reduction of Pt precursor to Pt. After 1 h the reactor was depressurized and purged with fresh $scCO_2$ (2–3 times the reactor volume) while the effluent was passed through an activated carbon packed bed cylinder before it was vented to the air. This typical deposition was repeated until the desired amount of Pt uptake is achieved.

For platinum and ceria co-deposition, tetrakis (2,2,6,6-tetramethyl 3,5-heptanedionato) cerium (IV) (Strem Chemicals, Newburyport, MA) was purchased and used as-received. Both the Pt and Ce precursors (0.05 mmol each) were placed inside the reactor and purged with N_2 as it was done for the platinum-only deposition. $scCO_2$ was charged to the reactor at 10.34 MPa and the wall temperature was then heated to 150 °C for 1 h, resulting in a pressure rise up to 19.58 MPa. The wall temperature was then reduced to 60 °C and $scCO_2$ was charged to the reactor to achieve a pressure of 17.24 MPa. A 200% molar excess of H_2 was then dosed into the reactor to induce the precursor reduction to metal. The reactor was depressurized and purged with fresh CO_2 following the similar sequences used for the Pt-only deposition. The intermediate heating step was necessary to ensure that the Ce precursor was fully dissolved in $scCO_2$.

We note that for the purposes of this study, only the anode layers are prepared via supercritical fluid deposition, whereas the cathode employed in fuel cell study is of the same Pt/C composition for all the experiments and was prepared via a conventional brush-paint method. One set of conventional Pt/C anode catalyst layer was fabricated via brush-paint method and tested in DMFC for comparison to the anodes prepared by SFD.

2.2. Physicochemical characterizations

The deposited films were analyzed by XPS using a Physical Instruments Quantum 2000 Scanning ESCA Microprobe (Physical Electronics, USA). The instrument was operated with monochromated Al Kα X-ray source (1486.6 eV), settings at 25 W, 15 kV and 100 μm beam size. The take-off angle was set at 45. For survey spectral acquisition (0–1000 eV), 187 eV pass energy was used with a step size of 1.6 eV, while for the multiplexes, 46 eV with 0.2 eV step size was used. For the sputter depth profiles, the samples were subject to 500 eV Ar^+ bombardment for 1 min on 1 mm × 1 mm area and the multiplex spectra were collected after every 1 min of sputtering for 20 cycles. The raw XPS data were analyzed using Multipak software (v. 6.1a Physical Electronics, USA), and the spectra were smoothened and fitted with least square method for the deconvolution procedure. All of the multiplex spectra were shifted according to the reference peak position of C1s at 284.5 eV. Each spectrum was fitted with an analytical function consisting of a sum of Gauss–Lorentzian shape functions for O1s and Ce3d, asymmetric peaks for Pt4f, with a Shirley base-line correction. X-ray diffractograms were recorded on a PANalytical X'Pert PRO X'Celerator using Ni filtered Cu Kα radiation (λ = 1.54187 Å). The data were collected with 2θ varying from 10 to 120, with an increment of 0.0167113°. X-ray generator voltage was 45 kV and the tube current was 40 mA. Scanning electron microscope (SEM) images and EDS mapping results were assessed by the use of a JEOL JSM 6480 LV equipped with an EDAX Genesis 2000 detector.

2.3. Electrochemical measurements

2.3.1. Half cell studies

The linear sweep and cyclic voltammetry studies were carried out in a conventional, airtight, three-electrode cell with Ag/AgCl as the reference electrode, platinum wire as the counter electrode and thin layers of Pt/C or Pt-Ceria/C catalyst system as a working electrode. The working electrode was prepared by mounting it on a Teflon platform such that it had an effective area of 0.196 cm^2 and it was exposed to an aqueous solution of 0.5 M H_2SO_4 and 1.0 M methanol. The tests were conducted at 25 °C at a scan rate of 20 mV s^{-1}. All the electrochemical measurements were carried out using a Potentiostat/Galvanostat model 263A EG & G Instruments (Princeton Applied Research). Prior to making measurements with

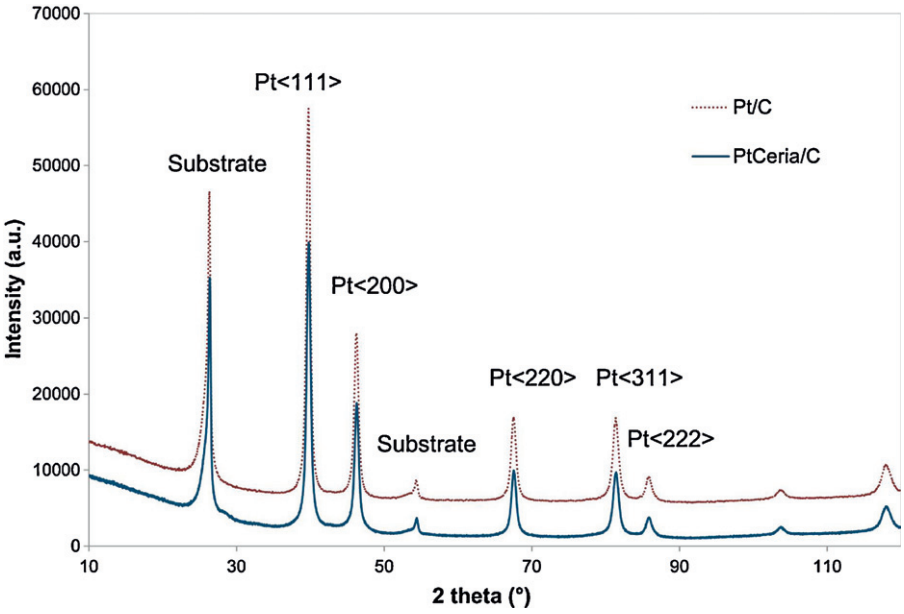

Fig. 2. X-ray diffractogram of representative Pt/C and Pt-Ceria/C samples prepared using supercritical fluid deposition.

cyclic voltammetry and chronoamperometry, the electrolyte was purged with N_2 gas for 30 min. Chronoamperometry data were collected for 1 h at 0.3 V vs. Ag/AgCl for the catalysts in a mixture of 0.5 M H_2SO_4 as electrolyte and 1.0 M methanol solution at 25 °C. Throughout the paper, the potential values are indicated in SHE scale. Water used for the experiments was previously distilled and pumped through a Nanopure system (Barnstead) to give 18 MΩ-cm nanopure water.

2.3.2. Single-cell testing

The thin layers of Pt/C or Pt-Ceria/C anode catalysts fabricated via SFD used for testing in fuel cell assembly are shown in Fig. 1b-I and b-II. Throughout the study, the Pt/C catalyst layers fabricated via conventional paint method has been employed as the cathodes (Fig. 1b-III).

A membrane electrode assembly (MEA) was fabricated by placing a Nafion® 117 membrane (Sigma–Aldrich) between a Pt or Pt-Ceria (3 mg-cm^{-2}) anode catalyst layer and a Pt (3 mg-cm^{-2}) cathode followed by hot-pressing at 160 °C, 7.5 MPa for 5 min. The MEAs had an effective area of 5 cm^2. All experiments, including the electrochemical measurements, were conducted with cells that consisted of an MEA sandwiched between two graphite flow-field plates. For all studies conducted in a fuel cell mode, 1.0 M methanol solution was pumped through the anode side at a flow rate of 2 ml/min and air to the cathode side at a flow rate of 200 sccm. The temperature and pressure of single cells were held at 25 or 60 °C and 0.101 MPa, respectively. Current–voltage curves were measured galvanostatically.

The linear sweep and cyclic voltammetry studies were conducted for the anode in the fuel cell mode by supplying 1.0 M methanol to the anode and the cathode Pt/C was supplied with a continuous stream of hydrogen (200 sccm) to make a standard hydrogen electrode (SHE).

The methanol cross-over studies were made in the fuel cell mode, by supplying 1.0 M methanol to the anode and the cathode Pt/C was supplied with nitrogen (200 sccm). Linear sweep voltammograms were made for the cathode to examine the extent of methanol permeated from anode to cathode side while employing different anode catalysts in the study.

3. Results and discussion

3.1. Supercritical fluid deposition of Pt and Pt-Ceria on GDL

Crystalline Pt and amorphous ceria were deposited on the GDL simultaneously using supercritical fluid deposition method. SFD of ceria using tetrakis (2,2,6,6-tetramethy 3,5-heptanedionato) cerium (IV) (Ce(tmhd)$_4$) typically occurs at temperatures above 250 °C [52,60]. However, co-deposition of Pt and ceria occurred at a temperature of 150 °C. These results are consistent with the observations of Zhang and Puddephatt who reported catalyst-enhanced chemical vapor deposition of yttrium oxide using palladium precursors as catalysts. In their work, the presence of Pd enabled the yttria deposition at a significantly lower temperature [61]. Although the mechanism of catalyst-enhanced chemical vapor deposition is not well understood, it is clear from our XRD and XPS results, discussed below, that the presence of Pt catalyzed ceria deposition at significantly lower temperatures.

The deposition of cubic phase Pt crystals during the preparation of Pt/C and Pt-Ceria/C was confirmed by X-ray diffraction (Fig. 2). Debye–Scherrer analysis on the Pt (1 1 1) peaks of the two samples yields an estimated Pt crystal size of 9 ± 1 nm. The diffraction patterns do not reveal the presence of CeO_2 nor Ce_2O_3. Mesguich et al. performed CeO_2 deposition in supercritical CO_2 at substrate temperatures of 250 and 300 °C. Their as-deposited films exhibited crystallinity, while XRD and XPS studies revealed that the deposited films were CeO_2 [60]. For this study, the deposition temperature is lower by 100 °C; therefore it is probable that the deposited ceria is amorphous.

XPS survey spectra (not shown) indicated the presence of Pt and C for Pt/C sample and Pt, Ce, O, and C for Pt-Ceria/C samples. The multiplex spectra of Pt4f, C1s, O1s and Ce3d are shown in Fig. 3 after 1 min sputtering with Ar^+ along with the results of curve fitting. Analysis of the Pt/C and Pt-Ceria/C samples both revealed Pt4f$_{7/2}$ (71.2 eV) and Pt4f$_{5/2}$ (74.5 eV) peaks (Fig. 3a and d). These binding energies for Pt are in good accordance with the literature values [62] indicating that the deposited Pt species are predominantly metallic. Pt/C sample did not show the O1s peak, whereas Pt-Ceria/C sample did show O1s spectra. This further supports that

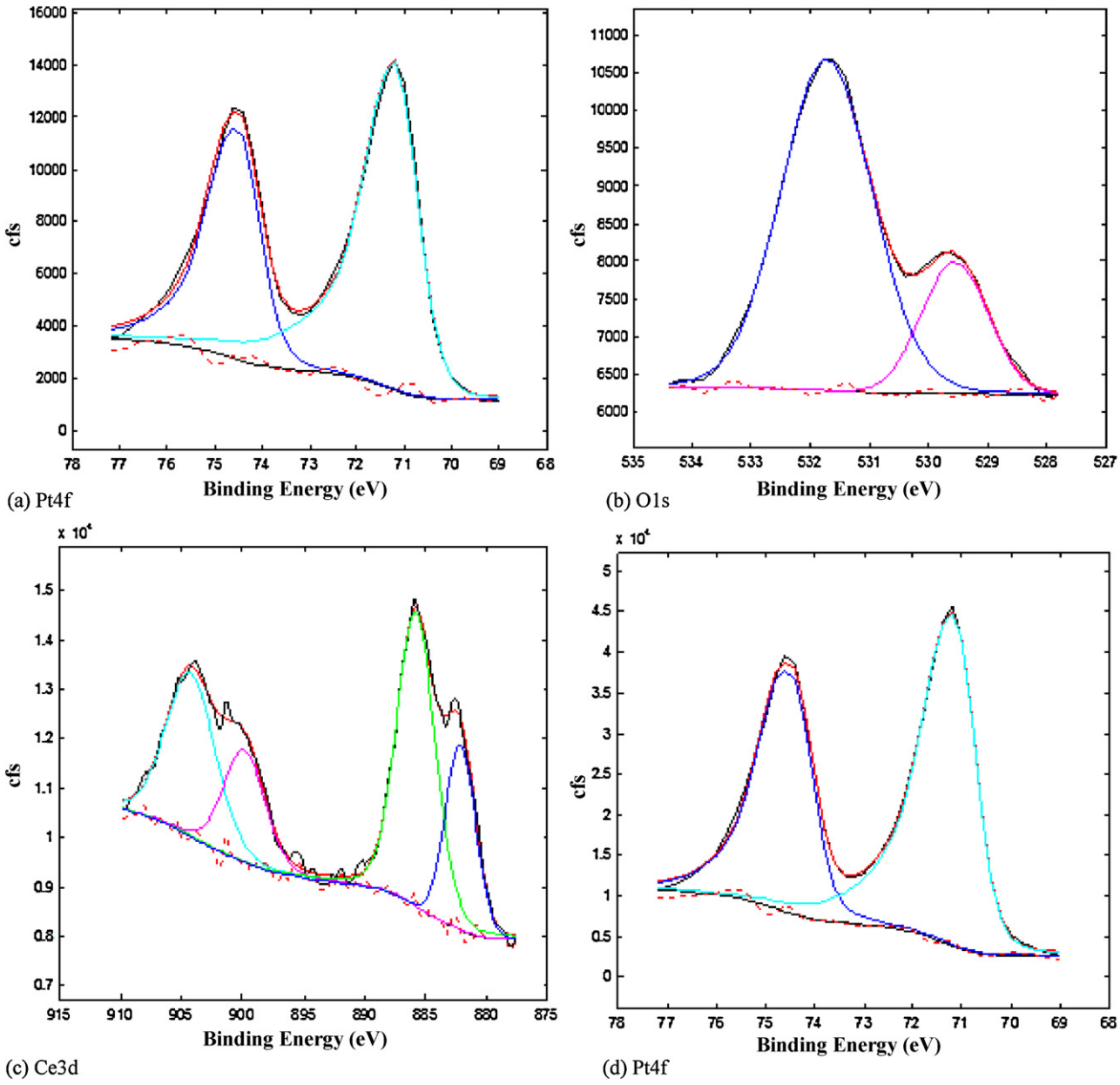

Fig. 3. De-convoluted XPS multiplex after 1 min Ar+ sputtering (a) Pt4f of Pt/C sample; (b) O1s, (c) Ce3d, (d) Pt4f of Pt-Ceria/C sample, they were prepared using supercritical fluid deposition.

the Pt layer deposited is pure metallic for Pt/C sample. The O1s peak was fitted with two major peaks centered at binding energies of 529.6 eV and 531.7 eV (Fig. 3b). The literature reports different values for O1s binding energy for cerium oxides; 530.4–530.7 eV [63], 530.0 eV [64], 529.5 eV [65], 529.2 eV [66], but it can be inferred that the deposited cerium is in oxide form. The XPS indicates that the oxidation state of ceria is predominantly Ce^{3+}, since it does not show the Ce^{4+} characteristic signal shapes. Mesguich et al. [60] observed as-deposited CeO_2 films exhibit Ce^{4+} characteristic Ce3d binding energy signal shapes on the surface and peaks attributed to Ce^{3+} after sputtering into the bulk. However, analysis of the Pt and ceria co-deposited sample suggests the presence of Ce^{3+} at the surface. The reduction of Ce^{4+} to Ce^{3+} can be caused by various means including Ar^+ sputtering, X-ray irradiation, and H_2 reduction [67]. The preparation of Pt-Ceria/C sample involved dosing H_2 to initiate the deposition of Pt. The presence of H_2 at the deposition conditions could result in the reduction of CeO_2 to Ce_2O_3. It is also possible that CeO_2 was reduced during the Ar^+ sputtering for XPS analysis. We further note that ceria can be re-oxidized by treatments with CO_2 [68] or methanol [69].

SEM characterization was carried out for the representative Pt/C sample (Fig. 4b) and Pt-Ceria/C sample (Fig. 4c) and both are compared to a blank electrode (carbon paper brush-painted with Vulcan) in Fig. 4a. The lighter areas in the SEM images are indicative of highly conductive material, presumably platinum. The electrodes are porous and catalyst particles are well dispersed on the gas diffusion layer. Recent investigations have shown that the porosity of the deposited material is critical to the electro-activity of the deposited materials in fuel cell applications [70]. Fig. 4c shows SEM and EDS element mapping of Pt and ceria in a representative Pt-Ceria/C sample. This result suggests that the SFD process maintains the desirable porous structure inherent to the GDL, although platinum and ceria were not uniformly distributed throughout the sample.

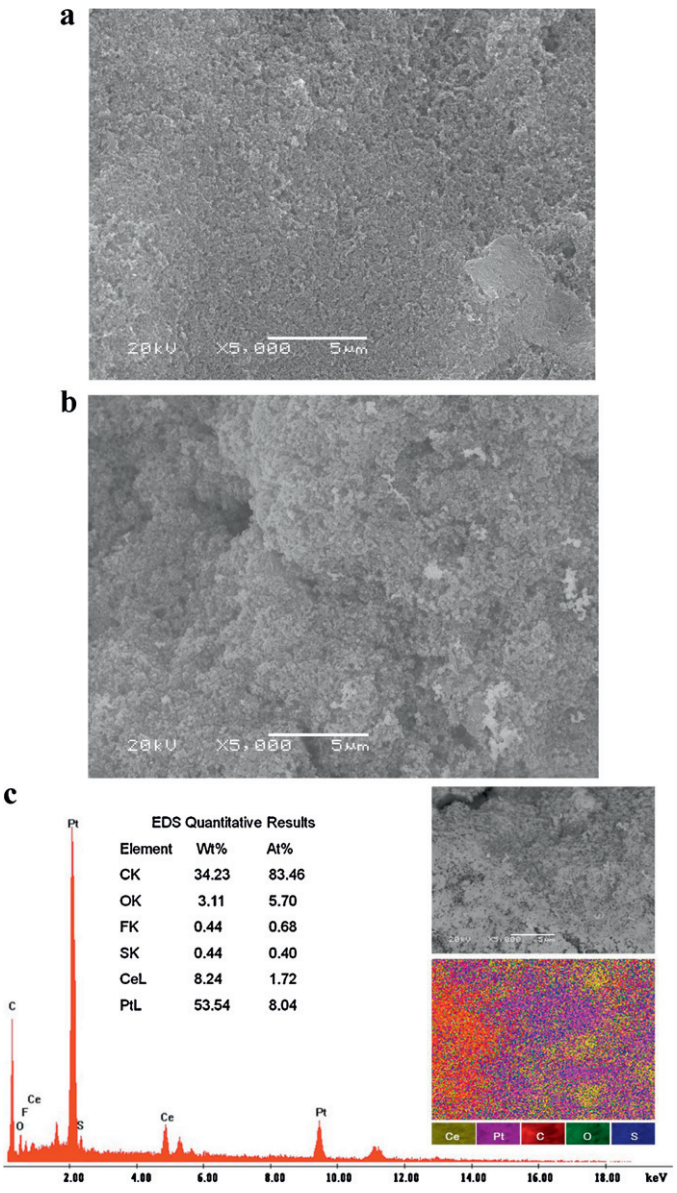

Fig. 4. (a) SEM image of a representative Pt/C sample, (b) SEM image of a gas diffusion layer (carbon paper coated with Vulcan), and (c) SEM-EDS results for a representative Pt-Ceria/C sample on which the supercritical fluid deposition is performed.

3.2. Half cell study of anodes prepared by SFD method

Thin layers of Pt/C or Pt-Ceria/C catalyst systems were subjected to electrochemical characterization by using cyclic voltammetry in 0.5 M H_2SO_4. The voltammogram shown in Fig. 5 clearly indicates the presence of platinum in both samples. The potential region between 0.3 and 0 V is due to hydrogen adsorption and desorption phenomenon on platinum, respectively, and the region between 0.6 and 0.85 V is due to PtO reduction. Adsorbed oxygen is reflected in the increase in oxidation current at about 0.80 V, and its reduction by a cathodic current peak at about 0.65 V in the reverse sweep [71,73].

The linear sweep voltammetry and cyclic voltammetric traces of Pt/C or Pt-Ceria/C catalyst systems made in aqueous solution of 0.5 M H_2SO_4 and 1.0 M methanol are shown in Figs. 6a and 6b respectively. From Fig. 6a, it can be seen clearly that the onset potential of Pt/C is 0.51 V vs. SHE with the peak current density of 77.28 mA cm^{-2}, while the onset potential of Pt-Ceria/C is 0.418 V

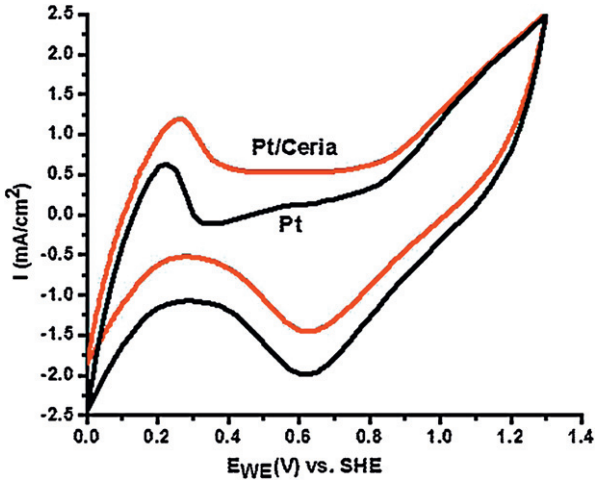

Fig. 5. Half-cell cyclic voltammetry of Pt/C or Pt-Ceria/C anode catalyst in 0.5 M H_2SO_4, at a scan rate of 20 mV s^{-1}.

vs. SHE with the peak current density of 101.18 mA cm^{-2}, indicating that the addition of ceria to platinum in the anode catalyst system enhances methanol oxidation activity.

Fig. 6b shows the cyclic voltammetry traces made for the thirtieth cycle. The Pt/C system exhibited a peak current density of 77.17 mA-cm^{-2} and the Pt-Ceria/C system showed a peak current density of 101.14 mA-cm^{-2}, indicating that the performance levels are maintained even after multiple cycles. It can be further noted that the reverse peak of Pt-Ceria/C is sharper and the peak current density is found at 0.935 V vs. SHE, while the – reverse peak of Pt/C is broader and the peak current density found at 0.855 V vs. SHE, indicating the facile removal of CO with the Pt-Ceria/C compared to Pt/C as anode catalyst system.

The chronoamperometric measurements are an effective method to evaluate the electrocatalytic activity and stability of the electrode material. Fig. 6c shows typical current density-time responses for methanol oxidation measured at a fixed potential of 0.5 V vs. SHE in 0.5 M H_2SO_4 aqueous solution containing 1.0 M methanol [72]. The Pt-Ceria/C catalyst system exhibited higher current densities throughout the testing time of 1 h, with comparable rates of decay in activity between Pt/C and Pt-Ceria/C catalyst systems.

3.3. DMFC fuel cell study with anodes prepared by SFD and paint methods

In order to examine the influence of fabrication techniques employed in catalyst layer formations on overall performance, single cell tests were conducted using a direct methanol fuel cell with Pt/C anode catalyst layers prepared using conventional paint methods (Fig. 1b-III) and compared with results for the thin layers prepared using SFD (Fig. 1b-I) under similar experimental conditions. The results are shown in Fig. 7. It can be seen that the DMFC single cell tests made with anode catalyst layers fabricated via SFD technique exhibited better performance both at room temperature and at 60 °C and compared to anode catalyst layers made by conventional route. This performance enhancement might arise from thinner anode catalyst layers, which would provide facile mass transfer of reactants to the active sites and the removal of the products, in addition to enhanced three phase boundary.

3.4. Anodes performance and fuel cross over tests in DMFC

The linear sweep and cyclic voltammetric traces of Pt/C or Pt-Ceria/C anode catalyst systems made in a direct methanol fuel cell

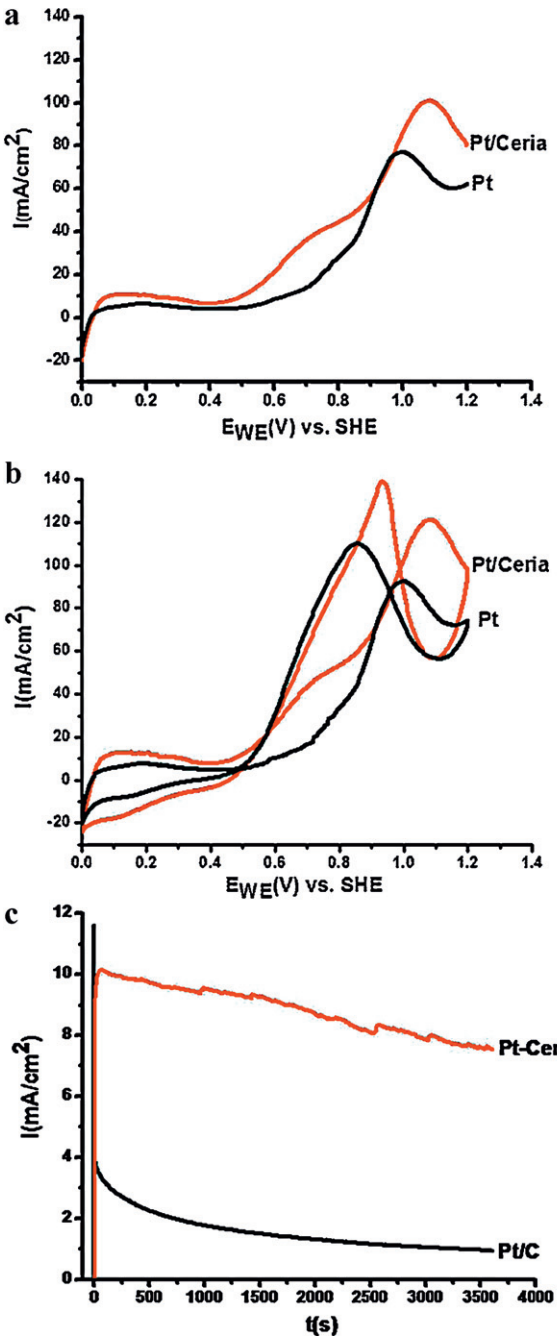

Fig. 6. Half-cell (a) linear sweep voltammetry, (b) cyclic voltammetry, and (c) chronoamperometric response of Pt/C or Pt-Ceria/C anode catalyst in 0.5 M H_2SO_4 and 1.0 M methanol at a scan rate of 20 mV s^{-1}. Chronoamperometry was done at 0.30 V vs. Ag/AgCl for 1 h.

mode by feeding 1.0 M methanol in the anode and 200 sccm hydrogen gas in the cathode side are shown in Fig. 8a and b, respectively. From Fig. 8a, it can be seen that the onset potential of Pt/C is 0.555 V vs. SHE with the peak current density of 37.6 mA cm^{-2}, while the onset potential of Pt-Ceria/C is 0.508 V vs. SHE with the peak current density of 74.6 mA cm^{-2}, indicating that the addition of ceria to platinum in anode catalyst system enhances the methanol oxidation activity. Fig. 8b shows the cyclic voltammetry traces made after 30 cycles. The Pt/C exhibited the peak current density of 33.26 mA cm^{-2}, and the Pt-Ceria/C shows a peak current density of 77.06 mA cm^{-2}, indicating that the performance levels are maintained after several cycling compared to the fresh linear sweep

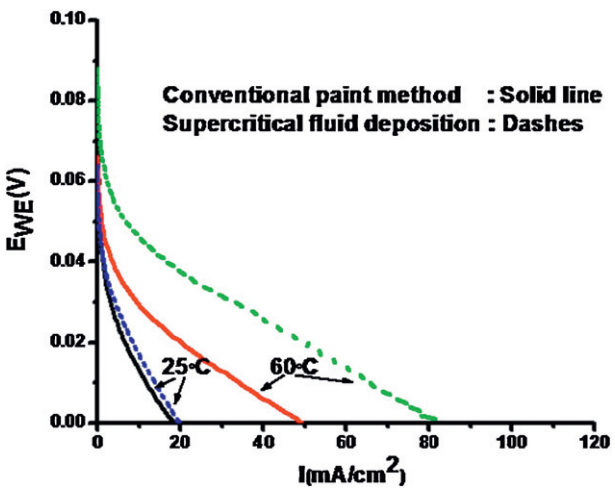

Fig. 7. Direct methanol fuel cell comparison of single cell test made with Pt/C electrodes fabricated through conventional paint method (solid line) and supercritical fluid deposition (dashes). Anode feed: 1.0 M methanol, 2.0 ml/min; cathode feed: air, 200 sccm; cell temperatures: 25 and 60 °C.

voltammetry traces made for these systems. These results are in agreement with the results from the half-cell studies (Fig. 6b). Further, the reverse peak of Pt-Ceria/C is sharper and the peak current density found at 0.853 V vs. SHE, while the slope of backward peak

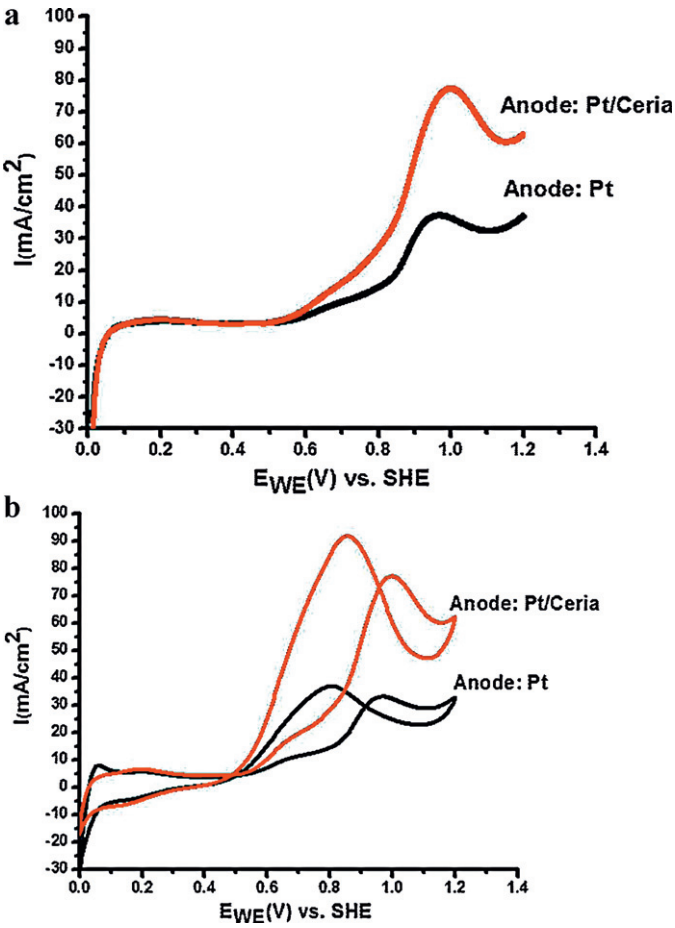

Fig. 8. Direct methanol fuel cell (a) linear sweep voltammetry and (b) cyclic voltammetry of Pt/C or Pt-Ceria/C anode catalyst in single cell mode with a H_2 cathode feed. Anode feed: 1.0 M methanol, 2.0 ml/min; cathode feed: H_2 gas, 200 sccm; cell temperature: 25 °C.

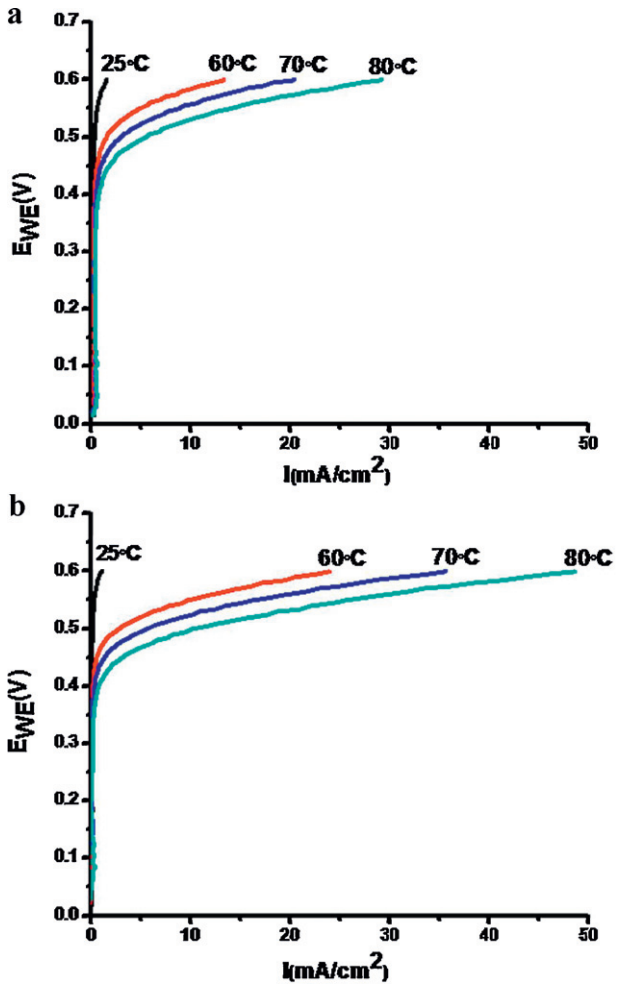

Fig. 9. Direct methanol fuel cell anode polarization curves of (a) Pt/C and (b) Pt-Ceria/C as anode catalyst in single cell mode with a H_2 cathode feed. Anode feed: 1.0 M methanol, 2.0 ml/min; cathode feed: H_2 gas, 200 sccm; cell temperatures: 25, 60, 70 and 80 °C.

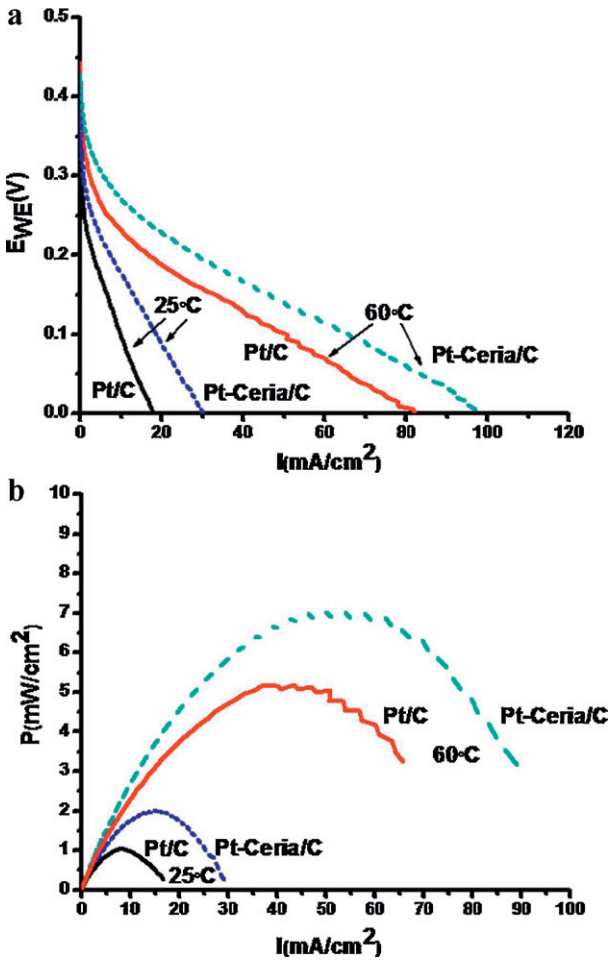

Fig. 10. Direct methanol fuel cell (a) current polarization and (b) power curves of Pt/C and Pt-Ceria/C as anode catalyst in single cell mode. Anode feed: 1.0 M methanol, 2.0 ml/min; cathode feed: air, 200 sccm; cell temperatures: 25 and 60 °C.

of Pt/C is steady and the peak current density found at 0.804 V vs. SHE, indicating the facile removal of CO with the Pt-Ceria/C anode catalyst system.

Anode polarization traces of Pt/C or Pt-Ceria/C anode catalyst systems were made in single cell assembly by feeding 1.0 M methanol in the anode and 200 sccm hydrogen gas in the cathode side at various cell temperatures such as 25, 60, 70 and 80 °C, Fig. 9a and b. It is found that at all temperatures of single cell operation studied; the Pt-Ceria/C catalyst system exhibited higher current density at any given potential.

The current-polarization and power curves for the direct methanol fuel cell were determined by supplying 1.0 M methanol to the anode and 200 sccm air at the cathode at two different operating temperatures 25 and 60 °C and the results are shown in Fig. 10. The tested anodes were Pt/C or Pt-Ceria/C anode catalyst systems prepared via SFD, while the cathode was Pt/C prepared via conventional paint method. As shown in Fig. 10a, the Pt/C system exhibited an open circuit voltage (OCV) of 0.403 V and 0.429 V at 25 and 60 °C, respectively. The Pt-Ceria/C anode catalyst systems exhibited a 0.410 V and 0.443 V at 25 and 60 °C, respectively. The higher OCV values shown by Pt-Ceria/C anode catalyst systems at both temperatures indicate its higher methanol oxidation activity, consequently leading to higher fuel utilization at the anode and lower methanol crossover. In addition, the power vs. current curves were made for the anodes Pt/C or Pt-Ceria/C at two different cell temperatures, 25 and 60 °C as given in Fig. 10b, showing that the Pt-Ceria/C anode catalyst system exhibited higher power at a given current at both cell temperatures.

The performance stability of the anodes Pt/C or Pt-Ceria/C in the direct methanol fuel cell-single cell assembly was tested and the

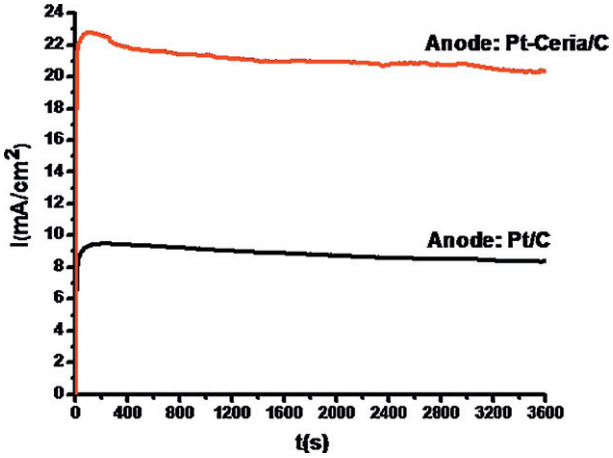

Fig. 11. Direct methanol fuel cell chronoamperometric traces of Pt/C or Pt-Ceria/C anode catalyst in direct methanol fuel cell under a constant applied cell voltage of 0.1 V for 1 h. Anode feed: 1.0 M methanol, 2.0 ml/min; cathode feed: air, 200 sccm; cell temperature: 25 °C. The cathode was used as a reference electrode, as well.

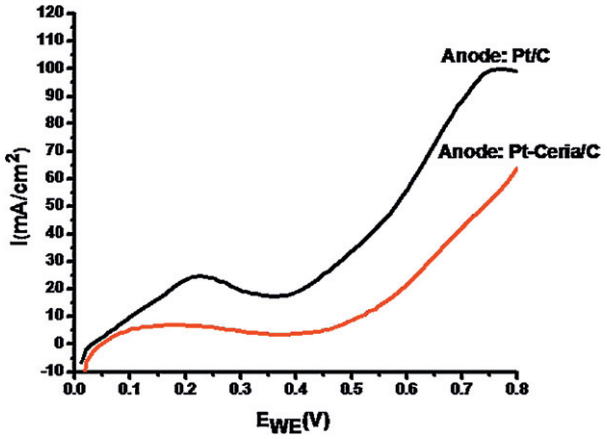

Fig. 12. Direct methanol fuel cell methanol cross over linear sweep voltammetry traces for Pt/C cathode, while employing Pt/C or Pt-Ceria/C anode catalyst. The anode was used as a reference electrode, as well. Anode feed: 1.0 M methanol, 2.0 ml/min; cathode feed: air, 200 sccm; cell temperature: 25 °C.

chronoamperometry traces were made under a constant applied cell voltage of 0.1 V for 1 h as shown in Fig. 11. The Pt-Ceria/C exhibited higher current density values that were nearly constant throughout the test period. A methanol cross over linear sweep voltammetry study was carried out at the cathode side by supplying 1.0 M methanol in the anode and the cathode was fed with stream of nitrogen gas with a flow rate of 200 sccm. These results are compared with the Pt/C anode catalyst under similar experimental conditions as shown in Fig. 12. The peak current density values are indicative of the extent of permeated methanol oxidation in the cathode side. It can be seen that while employing Pt-Ceria/C as the anode catalyst, the permeated methanol is decreased and hence, lower current density values were found, whereas with Pt/C as the anode catalyst there is a higher extent of permeated methanol. This could be indicative of better catalytic activity of Pt-Ceria/C toward methanol oxidation at the anode side, thus enhancing the fuel utilization, thereby restricting the methanol permeation.

4. Conclusion

Supercritical fluid deposition (SFD) was utilized to deposit Pt and ceria simultaneously to construct the fuel cell anode for a direct methanol fuel cell system and for the study of the methanol oxidation process. It was found that Pt catalyzes the deposition of ceria and allows for co-deposition at a reduced temperature as low as 60 °C. The deposited Pt was predominantly metallic and crystalline with estimated grain size of 9 nm. The thin layer electrode formed via supercritical fluid deposition exhibited higher performance in fuel cell operations compared to electrodes prepared with a conventional way of coating the gas diffusion layers by the brush and paint method when Pt/C was employed as anode catalyst. Further, the Pt-ceria catalyst deposited by SFD exhibited higher methanol oxidation activity compared to the platinum catalyst alone. Thus, both the method of deposition as well as control of composition are important factors. The linear sweep traces of the cathode made for the methanol cross over study indicate that Pt-Ceria/C as the anode catalyst, due to its better activity for methanol, improves the fuel utilization, minimizing the methanol permeation from anode to cathode compartment. Studies are underway, to improve the three phase boundary by the further optimization of the deposition technique and fabrication of membrane electrode assembly to realize improved DMFC performance. The current study has primarily focused on directly depositing Pt and ceria onto the carbon paper (GDL). However, with the current SFD approach it will be feasible to deposit these catalysts to the carbon nanotube or other mesoporous carbon nanoparticles prior to fabrication of the GDL using conventional techniques.

Acknowledgments

This work was supported by the NSF Center for Hierarchical Manufacturing at the University of Massachusetts (CMMI-0531171) and by NASA URC Center for Advanced Nanoscale Materials (NNX10AQ17A). This material is based upon work supported in part by, the U.S. Army Research Office under grant number 54635CH. Eunyoung You and Rolando Guzmán-Blas equally contributed to this work.

References

[1] B. Viswanathan, M.A. Scibioh, Fuel Cells: Principles and Applications, CRC Press, Taylor and Francis Group, New York, 2007.
[2] M.A. Scibioh, B. Rajesh, B. Viswanathan, Proceedings of the Indian National Science Academy Part A 68 (2002) 99.
[3] G.T. Burstein, C.J. Barnett, A.R. Kucernak, K.R. Williams, Catalysis Today 38 (1997) 425.
[4] A. Hamnett, Catalysis Today 38 (1997) 445.
[5] E. Antolini, Materials Chemistry and Physics 78 (2003) 563.
[6] C. Bock, C. Paquet, M. Couillard, G.A. Botton, B.R. MacDougall, Journal of the American Chemical Society 126 (2004) 8028.
[7] G.A. Camara, M.J. Giz, V.A. Paganin, E.A. Ticianelli, Journal of Electroanalytical Chemistry 537 (2002) 21.
[8] P. Costamagna, S. Srinivasan, Journal of Power Sources 102 (2001) 242.
[9] H.A. Gasteiger, N. Markovic, P.N. Ross, E.J. Cairns, Journal of Physical Chemistry 98 (1994) 617.
[10] V. Radmilovic, H.A. Gasteiger, P.N. Ross, Journal of Catalysis 154 (1995) 98.
[11] M. Götz, H. Wendt, Electrochimica Acta 43 (1998) 3637.
[12] G. Samjeske, H. Wang, T. Löffler, H. Baltruschat, Electrochimica Acta 47 (2002) 3681.
[13] P.K. Shen, K.Y. Chen, A.C.C. Tseung, Journal of the Electrochemical Society 142 (1995) 85.
[14] H.R. Colón-Mercado, H. Kim, B.N. Popov, Electrochemistry Communications 6 (2004) 795.
[15] T.C. Deivaraj, W. Chen, J.Y. Lee, Journal of Materials Chemistry 13 (2003) 2555.
[16] K.W. Park, J.H. Choi, B.K. Kwon, S.A. Lee, Y.E. Sung, H.Y. Ha, S.A. Hong, H. Kim, A. Wieckowski, Journal of Physical Chemistry B 106 (2002) 1869.
[17] D.C. Papageorgopoulos, M. Keijzer, F.A. De Bruijn, Electrochimica Acta 48 (2002) 197.
[18] K.-W. Park, J.-H. Choi, K.-S. Ahn, Y.-E. Sung, Journal of Physical Chemistry B 108 (2004) 5989.
[19] Z. Jusys, T.J. Schmidt, L. Dubau, K. Lasch, L. Jörissen, J. Garche, R.J. Behm, Journal of Power Sources 105 (2002) 297.
[20] K. Lasch, L. Jörissen, J. Garche, Journal of Power Sources 84 (1999) 225.
[21] L.X. Yang, C. Bock, B. MacDougall, J. Park, Journal of Applied Electrochemistry 34 (2004) 427.
[22] C.H. Park, M.A. Scibioh, H.J. Kim, I.H. Oh, S.A. Hong, H.Y. Ha, Journal of Power Sources 162 (2006) 1023.
[23] M.A. Scibioh, S.-K. Kim, E.A. Cho, T.-H. Lim, S.-A. Hong, H.Y. Ha, Applied Catalysis B: Environmental 84 (2008) 773.
[24] A. Bauer, C.W. Oloman, E.L. Gyenge, Journal of Power Sources 193 (2009) 754.
[25] S. Litster, G. McLean, Journal of Power Sources 130 (2004) 61.
[26] A.M. Zainoodin, S.K. Kamarudin, W.R.W. Daud, International Journal of Hydrogen Energy 35 (2010) 4606.
[27] H.B. Yu, J.H. Kim, H.I. Lee, M.A. Scibioh, J. Lee, J. Han, S.P. Yoon, H.Y. Ha, Journal of Power Sources 140 (2005) 59.
[28] C. Xu, P.K. Shen, Chemical Communications 2004 (2004) 2238.
[29] C. Xu, P.K. Shen, Journal of Power Sources 142 (2005) 27.
[30] C.L. Campos, C. Roldán, M. Aponte, Y. Ishikawa, C.R. Cabrera, Journal of Electroanalytical Chemistry 581 (2005) 206.
[31] J.W. Guo, T.S. Zhao, J. Prabhuram, R. Chen, C.W. Wong, Journal of Power Sources 156 (2006) 345.
[32] A.H. Romang, J.J. Watkins, Chemical Reviews 110 (2010) 459.
[33] J.M. Blackburn, D.P. Long, A. Cabanas, J.J. Watkins, Science 294 (2001) 141.
[34] B. Zhao, T. Momose, T. Ohkubo, Y. Shimogaki, Microelectronic Engineering 85 (2008) 675.
[35] A. Cabañas, D.P. Long, J.J. Watkins, Chemistry of Materials 16 (2004) 2028.
[36] D.P. Long, J.M. Blackburn, J.J. Watkins, Advanced Materials 12 (2000) 913.
[37] E.T. Hunde, J.J. Watkins, Chemistry of Materials 16 (2004) 498.
[38] A. Cabañas, X. Shan, J.J. Watkins, Chemistry of Materials 15 (2003) 2910.
[39] E. Kondoh, Japanese Journal of Applied Physics 43 (2004) 3928.
[40] E. Kondoh, K. Shigama, Thin Solid Films 491 (2005) 228.
[41] M. Matsubara, M. Hirose, K. Tamai, Y. Shimogaki, E. Kondoh, Journal of the Electrochemical Society 156 (2009) H443.
[42] Y. Zong, J.J. Watkins, Chemistry of Materials 17 (2005) 560.
[43] Q. Peng, J.C. Spagnola, G.N. Parsons, Journal of the Electrochemical Society 155 (2008) D580.

[44] J.M. Blackburn, D.P. Long, J.J. Watkins, Chemistry of Materials 12 (2000) 2625.
[45] N.E. Fernandes, S.M. Fisher, J.C. Poshusta, D.G. Vlachos, M. Tsapatsis, J.J. Watkins, Chemistry of Materials 13 (2001) 2023.
[46] C.S. Lin, F.L.Y. Lam, X. Hu, W.Y. Tam, K.M. Ng, Journal of Physical Chemistry C 112 (2008) 10068.
[47] J.J. Watkins, J.M. Blackburn, T.J. McCarthy, Chemistry of Materials 11 (1999) 213.
[48] C.F. Karanikas, J.J. Watkins, Microelectronic Engineering 87 (2010) 566.
[49] A. O'Neil, J.J. Watkins, Chemistry of Materials 18 (2006) 5652.
[50] T. Gougousi, D. Barua, E.D. Young, G.N. Parsons, Chemistry of Materials 17 (2005) 5093.
[51] Q. Peng, D. Hojo, K.J. Park, G.N. Parsons, Thin Solid Films 516 (2008) 4997.
[52] A. O'Neil, J.J. Watkins, Chemistry of Materials 19 (2007) 5460.
[53] H. Uchida, A. Otsubo, K. Itatani, S. Koda, Japanese Journal of Applied Physics 44 (2005) 1901.
[54] T. Gougousi, Z. Chen, Thin Solid Films 516 (2008) 6197.
[55] Y. Lin, X. Cui, C. Yen, C.M. Wai, Journal of Physical Chemistry B 109 (2005) 14410.
[56] Y. Lin, X. Cui, C.H. Yen, C.M. Wai, Langmuir 21 (2005) 11474.
[57] G. An, P. Yu, L. Mao, Z. Sun, Z. Liu, S. Miao, Z. Miao, K. Ding, Carbon 45 (2007) 536.
[58] R. Jiang, Y. Zhang, S. Swier, X. Wei, C. Erkey, H.R. Kunz, J.M. Fenton, Electrochemical and Solid-State Letters 8 (2005) A611.
[59] O. Aschenbrenner, S. Kemper, N. Dahmen, K. Schaber, E. Dinjus, Journal of Supercritical Fluids 41 (2007) 179.
[60] D. Mesguich, C. Aymonier, J.M. Bassat, F. Mauvy, E. You, J.J. Watkins, Chemistry of Materials 23 (2011) 5323.
[61] Y. Zhang, R.J. Puddephatt, Chemistry of Materials 11 (1999) 148.
[62] J.F. Moulder, J. Chastain, Handbook of X-ray Photoelectron Spectroscopy, Perkin-Elmer, Eden Prairie, MN, 1992.
[63] D.R. Mullins, S.H. Overbury, D.R. Huntley, Surface Science 409 (1998) 307.
[64] P. Concepción, A. Corma, J. Silvestre-Albero, V. Franco, J.Y. Chane-Ching, Journal of the American Chemical Society 126 (2004) 5523.
[65] J.P. Holgado, G. Munuera, J.P. Espinós, A.R. González-Elipe, Applied Surface Science 158 (2000) 164.
[66] D. Barreca, G.A. Battiston, R. Gerbasi, E. Tondello, Surface Science Spectra 7 (2000) 297.
[67] L. Qiu, F. Liu, L. Zhao, Y. Ma, J. Yao, Applied Surface Science 252 (2006) 4931.
[68] T. Staudt, Y. Lykhach, N. Tsud, T. Skála, K. Prince, V. Matolín, J. Libuda, Journal of Catalysis 275 (2010) 181.
[69] C. Binet, A. Badri, J.C. Lavalley, Journal of Physical Chemistry 98 (1994) 6392.
[70] S.K. Natarajan, J. Hamelin, Journal of Power Sources 195 (2010) 7574.
[71] Z. Liu, L. Ming Gan, L. Hong, W. Chen, J. Yang Lee, Journal of Power Sources 139 (2005) 73.
[72] G.Q. Lu, W. Chrzanowski, A. Wieckowski, Journal of Physical Chemistry B 104 (2000) 5566.
[73] S. Patra, N. Munichandraiah, Langmuir 25 (2009) 1732.
[74] H. Yuan, D. Guo, X. Qiu, W. Zhu, L. Chen, Journal of Power Sources 188 (2009) 8.
[75] Z.C. Tang, G.X. Lu, Applied Catalysis B: Environmental 79 (2008) 1.
[76] E. Lee, A. Manthiram, Journal of Physical Chemistry C 114 (2010) 21833.